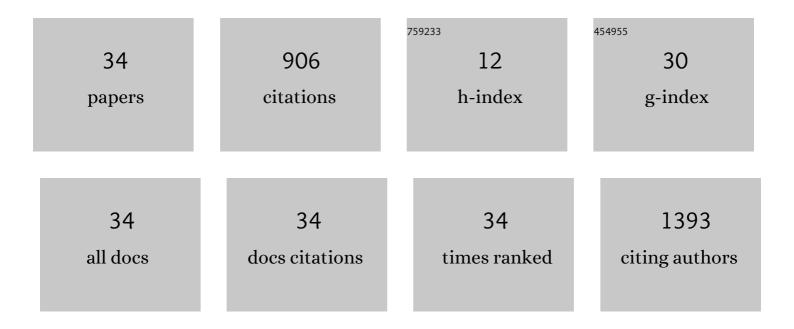


## List of Publications by Year in descending order

Source: https://exaly.com/author-pdf/4380618/publications.pdf Version: 2024-02-01



ΟιΝΟ ΖΗΛΟ

#	Article	IF	CITATIONS
1	A Multigrid InSAR Technique for Joint Analyses at Single-Look and Multi-Look Scales. IEEE Geoscience and Remote Sensing Letters, 2022, 19, 1-5.	3.1	6
2	Changes of Chinese Coastal Regions Induced by Land Reclamation as Revealed through TanDEM-X DEM and InSAR Analyses. Remote Sensing, 2022, 14, 637.	4.0	6
3	Multi-GNSS Fast Precise Point Positioning with Multi-Frequency Uncombined Model and Cascading Ambiguity Resolution. Mathematical Problems in Engineering, 2022, 2022, 1-16.	1.1	6
4	Ambiguity Resolution for Long Baseline in a Network with BDS-3 Quad-Frequency Ionosphere-Weighted Model. Remote Sensing, 2022, 14, 1654.	4.0	7
5	On the Exploitation of Remote Sensing Technologies for the Monitoring of Coastal and River Delta Regions. Remote Sensing, 2022, 14, 2384.	4.0	6
6	A Multi-Station Troposphere Modelling Method Based on Error Compensation Considering the Influence of Height Factor. Journal of Navigation, 2021, 74, 38-59.	1.7	3
7	The activation of methane by Ni-Cu/MoOx for the synthesis of ethanol. Journal of Chemical Sciences, 2021, 133, 1.	1.5	2
8	Assessment of Quad-Frequency Long-Baseline Positioning with BeiDou-3 and Galileo Observations. Remote Sensing, 2021, 13, 1551.	4.0	7
9	An Improved Multipath Mitigation Method and Its Application in Real-Time Bridge Deformation Monitoring. Remote Sensing, 2021, 13, 2259.	4.0	2
10	Performance of Single-Epoch EWL/WL/NL Ambiguity-Fixed Precise Point Positioning with Regional Atmosphere Modelling. Remote Sensing, 2021, 13, 3758.	4.0	4
11	Characteristics and modelling of BDS satellite inter-frequency clock bias for triple-frequency PPP. Survey Review, 2020, 52, 38-48.	1.2	4
12	CeZrOx Promoted Water-Gas Shift Reaction under Steam–Methane Reforming Conditions on Ni-HTASO5. Catalysts, 2020, 10, 1110.	3.5	3
13	On the Characterization and Forecasting of Ground Displacements of Ocean-Reclaimed Lands. Remote Sensing, 2020, 12, 2971.	4.0	8
14	Anomaly Detection for Urban Vehicle GNSS Observation with a Hybrid Machine Learning System. Remote Sensing, 2020, 12, 971.	4.0	13
15	One-Step Synthesis of Highly Active and Stable Ni–ZrO <sub><i>x</i></sub> for Dry Reforming of Methane. Industrial & Engineering Chemistry Research, 2020, 59, 11441-11452.	3.7	46
16	Loss of the voltage-gated proton channel Hv1 decreases insulin secretion and leads to hyperglycemia and glucose intolerance in mice. Journal of Biological Chemistry, 2020, 295, 3601-3613.	3.4	10
17	Lattice structure and microwave dielectric properties of La[Al 1â^' x (Mg 0.5 Ti 0.5 ) x ]O 3 ( x Â=Â0â€0.2)â€basec ceramics. Journal of the American Ceramic Society, 2020, 103, 3231-3237.	3.8	13
18	Increased expression of SLC46A3 to oppose the progression of hepatocellular carcinoma and its effect on sorafenib therapy. Biomedicine and Pharmacotherapy, 2019, 114, 108864.	5.6	22

QING ZHAO

#	Article	IF	CITATIONS
19	Proton pump inhibitors have pH-dependent effects on the thermostability of the carboxyl-terminal domain of voltage-gated proton channel Hv1. European Biophysics Journal, 2018, 47, 237-247.	2.2	1
20	On the Effects of InSAR Temporal Decorrelation and Its Implications for Land Cover Classification: The Case of the Ocean-Reclaimed Lands of the Shanghai Megacity. Sensors, 2018, 18, 2939.	3.8	12
21	An Alternative to Lithium Metal Anodes: Nonâ€dendritic and Highly Reversible Sodium Metal Anodes for Li–Na Hybrid Batteries. Angewandte Chemie - International Edition, 2018, 57, 14796-14800.	13.8	102
22	An Alternative to Lithium Metal Anodes: Nonâ€dendritic and Highly Reversible Sodium Metal Anodes for Li–Na Hybrid Batteries. Angewandte Chemie, 2018, 130, 15012-15016.	2.0	14
23	Low-Temperature Catalytic CO <sub>2</sub> Dry Reforming of Methane on Ni-Si/ZrO <sub>2</sub> Catalyst. ACS Catalysis, 2018, 8, 6495-6506.	11.2	220
24	Two benzaldehyde derivatives and their artefacts from a gorgonian-derived <i>Eurotium</i> sp. fungus. Natural Product Research, 2017, 31, 268-274.	1.8	7
25	The 2015–2016 Ground Displacements of the Shanghai Coastal Area Inferred from a Combined COSMO-SkyMed/Sentinel-1 DInSAR Analysis. Remote Sensing, 2017, 9, 1194.	4.0	28
26	The Use of C-/X-Band Time-Gapped SAR Data and Geotechnical Models for the Study of Shanghai's Ocean-Reclaimed Lands through the SBAS-DInSAR Technique. Remote Sensing, 2016, 8, 911.	4.0	63
27	Rechargeable Roomâ€Temperature Na–CO <sub>2</sub> Batteries. Angewandte Chemie - International Edition, 2016, 55, 6482-6486.	13.8	202
28	Cyclic utilization of HP-β-CD in the bioconversion of cortisone acetate by Arthrobacter simplex. Biotechnology Letters, 2016, 38, 597-602.	2.2	5
29	The voltage-gated proton channel Hv1 is expressed in pancreatic islet $\hat{I}^2$ -cells and regulates insulin secretion. Biochemical and Biophysical Research Communications, 2015, 468, 746-751.	2.1	15
30	The pH-sensitive structure of the C-terminal domain of voltage-gated proton channel and the thermodynamic characteristics of Zn2+ binding to this domain. Biochemical and Biophysical Research Communications, 2015, 456, 207-212.	2.1	4
31	Deepâ€water seamount wakes on SEASAT SAR image in the Gulf Stream region. Geophysical Research Letters, 2012, 39, .	4.0	20
32	Shear-flow induced secondary circulation in parallel underwater topographic corrugation and its application to satellite image interpretation. Journal of Ocean University of China, 2012, 11, 427-435.	1.2	9
33	InSAR detection of residual settlement of an ocean reclamation engineering project: a case study of Hong Kong International Airport. Journal of Oceanography, 2011, 67, 415-426.	1.7	34
34	Effects of Cu Addition on Microstructure and Adhesion Properties of Ti-Al-N Nanocomposite Films Deposited by Magnetron Sputtering. Advanced Materials Research, 0, 652-654, 1751-1754.	0.3	2